JACS
JOURNAL OF THE AMERICAN CHEMICAL SOCIETY
Article
pubs.acs.org/JACS

Disproportionation in Li−O_2 Batteries Based on a Large Surface Area Carbon Cathode

Dengyun Zhai,[†] Hsien-Hau Wang,[‡] Junbing Yang,[†] Kah Chun Lau,[‡] Kaixi Li,[§] Khalil Amine,*[,†,#] and Larry A. Curtiss*[,‡]

[†]Chemical Sciences and Engineering Division, Argonne National Laboratory, Argonne, Illinois 60439, United States
[‡]Materials Science Division, Argonne National Laboratory, Argonne, Illinois 60439, United States
[§]Key Laboratory of Carbon Materials, Institute of Coal Chemistry, Chinese Academy of Sciences, Taiyuan, Shanxi 030001, PR China
[#]King Abdulazi University, Jeddah 21589, Saudi Arabia

Supporting Information

ABSTRACT: In this paper we report on a kinetics study of the discharge process and its relationship to the charge overpotential in a Li−O_2 cell for large surface area cathode material. The kinetics study reveals evidence for a first-order disproportionation reaction during discharge from an oxygen-rich Li_2O_2 component with superoxide-like character to a Li_2O_2 component. The oxygen-rich superoxide-like component has a much smaller potential during charge (3.2−3.5 V) than the Li_2O_2 component (~4.2 V). The formation of the superoxide-like component is likely due to the porosity of the activated carbon used in the Li−O_2 cell cathode that provides a good environment for growth during discharge. The discharge product containing these two components is characterized by toroids, which are assemblies of nanoparticles. The morphologic growth and decomposition process of the toroids during the reversible discharge/charge process was observed by scanning electron microscopy and is consistent with the presence of the two components in the discharge product. The results of this study provide new insight into how growth conditions control the nature of discharge product, which can be used to achieve improved performance in Li−O_2 cell.

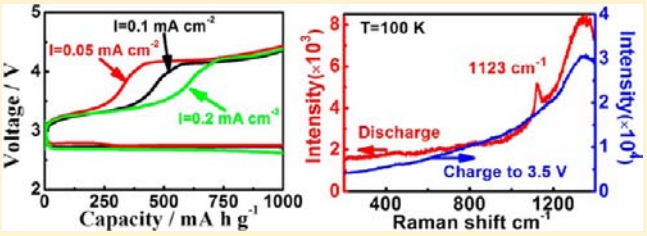

1. INTRODUCTION

In recent years, rechargeable lithium−oxygen (Li−O_2) batteries have attracted much interest as their theoretical energy density is far higher than that of lithium-ion batteries.[1−4] Typical nonaqueous Li−O_2 batteries consist of a lithium metal anode, a separator, a carbon-based cathode, and organic electrolyte in an oxygen-filled cell. Li−O_2 batteries still have quite a few challenges to overcome, such as large voltage charge overpotentials, decomposition of electrolytes, poor cycle life, and so on. Ether-based electrolytes are considered more stable than carbonate-based electrolytes, although the ether-based electrolyte can also decompose during discharge.[3,5−12] Different kinds of carbon materials as the cathode materials have been tested for Li−O_2 batteries.[3,8,9,13−15] Yang et al. synthesized carbon nanofibers on porous alumina and used them for Li−O_2 batteries and first found toroid-shape Li_2O_2 particles.[3] Jung and co-workers adopted super P, a different kind of carbon black, as the cathode of Li−O_2 coin-cell and exhibited good cycle life performance in a time-controlled mode.[7] Several researchers introduced catalysts (metal oxide or metal nanoparticles) into the cathode, aimed at reducing the overpotentials, especially for the charge cycle.[9,16−19] Recently, Bruce et al. reported that a Li−O_2 cell composed of a dimethyl sulfoxide-based electrolyte and nanoporous gold electrode can retain 95% of its controlled capacity after 100 cycles.[13,20]

One of the unresolved questions involving Li−O_2 batteries is the mechanism of the oxygen reduction reaction. During discharge, O_2 is reduced on the cathode (oxygen reduction reaction, ORR) to form lithium peroxide (Li_2O_2). One possibility is that the lithium peroxide is formed from two sequential electron transfer steps.

$$O_2 + Li^+ + e^- \rightarrow LiO_2 \quad (1)$$

$$LiO_2 + Li^+ + e^- \rightarrow Li_2O_2 \quad (2)$$

There is some kinetics and theoretical evidence to support this type of mechanism.[21,22] An alternative route to Li_2O_2 involves a one-electron reaction followed by disproportionation via LiO_2.[2,23−25]

$$O_2 + e^- \rightarrow O_2^- \quad (3)$$

$$O_2^- + Li^+ \rightarrow LiO_2 \quad (4)$$

$$2LiO_2 \rightarrow Li_2O_2 + O_2 \quad (5)$$

There is some evidence for this from surface enhanced raman spectroscopy (SERS) studies on a Au electrode that indicates O_2 is first reduced to superoxide anion (O_2^-) through a one-

Received: April 5, 2013
Published: September 20, 2013

   dx.doi.org/10.1021/ja403199d | J. Am. Chem. Soc. 2013, 135, 15364−15372

electron transfer process and Li cation complexation (eqs 3 and 4) to form lithium superoxide (LiO_2), which then disproportionates to form Li_2O_2 and O_2 (eq 5).[2] Other evidence comes from Nazar et al.[1] who have shown that adding superoxide anion by itself to a TEGDME/$LiPF_6$ solution results in O_2 evolution and X-ray diffraction (XRD) shows that Li_2O_2 is formed. However, there is much that is still unknown about the disproportionation reaction in Li−O_2 discharge chemistry, such as how it affects morphology of the discharge product and the charge chemistry.

In this work we report on an investigation of a Li−O_2 cell based on a large surface area carbon cathode to gain more insight into the existence of the LiO_2 disproportionation reaction during discharge and the role it may play in the nature of the discharge product and subsequent charge potential. In a previous study on activated carbon (AC) with a surface area up to 3840 m^2 g^{-1}, we reported magnetic and spectroscopic evidence for a lithium superoxide-like species in the discharge product that was consistent with predictions from density functional calculations on lithium peroxide clusters and surfaces.[26−28] Because of this identification of the lithium superoxide-like species in the discharge product, the activated carbon cathode material provides an excellent opportunity to investigate the disproportionation reaction. The investigation reported in this paper reveals that a disproportionation reaction results in two components of the discharge product, a Li_2O_2 component and an oxygen-rich superoxide-like component, that are responsible for two plateaus observed during charging. In the second section, we describe the experimental methods used. In the third section, we describe a kinetics analysis of the charge/discharge data as a function of the discharge capacity and current density to help understand the discharge reaction mechanism. In addition, the morphology changes of the lithium peroxide material during discharge and charge are presented and reveal interesting differences in the two processes that provide further evidence for the importance of the disproportionation reaction in the Li−O_2 cell. Finally, we discuss how the properties of the activated carbon cathodes may be used in future Li−O_2 studies.

2. EXPERIMENTAL METHODS

The AC was prepared by mixing 4 g of petroleum coke with 20 g of potassium hydroxide (KOH) and heating under argon flow. The heat treatment was carried out at a rate of 5 °C min^{-1}, and the mixture was held at 830 °C for 90 min and cooled. The resulting mixture was washed with distilled water, until the pH value reached 6−7, and filtered. Finally, the as-prepared AC powders were dried at 85 °C under a vacuum for 48 h, followed by grinding and sieving to a particle size less than 40 μm. An analysis of the impurities in the AC was performed in our previous study both before and after acid treatment.[26] After acid treatment, the only impurity remaining to any extent was potassium. The two samples, treated and untreated, gave similar voltage profiles. The potassium K content in the activated carbon based on X-ray fluorescence analysis is at the level of 1410 ppm or 0.14%. This low level of K precludes the possibility that observed superoxide-like component (Section III) in the Li discharge process is KO_2.

The specific surface area of the AC was determined by nitrogen gas adsorption at 77 K.[26] An automated adsorption apparatus (Micromeritics ASAP 2020) was employed for these measurements. The surface area was determined from the Brunauer−Emmett−Teller (BET) method and the pore size distribution by density function theory (DFT).[29] The electrode was first washed with TEGDME solvent and dried at 80 °C under a vacuum in the glovebox, and then the dried electrode was characterized by XRD. The XRD patterns were obtained by using a diffractometer (Miniflex, Rigaku Corp.) in which Cu Kα (λ = 0.154 nm) was used as the radiation source. The morphology of AC electrode was also observed using a field-emission scanning electron microscope (SEM Hitachi S-4700) equipped with energy dispersive X-ray (EDX) spectroscopy. Raman spectra of discharged cathode were obtained using a Renishaw inVia microscope spectrometer. The sample was loaded inside of a glovebox to a gastight Raman cell with glass or quartz window.

Electrochemical measurements were carried out in plastic Swagelok cells.[26,30] AC powders (80 wt %) and polyvinylidene fluoride binder (PVDF, 20 wt %) were mixed in a solution of *N*-methyl-2-pyrrolidone (NMP) and coated on Torray carbon paper. The carbon loading density was about 1.6 mg cm^{-2}. The anode, electrolyte, and separator were lithium metal foil, 1.0 M $LiCF_3SO_3$ in TEGDME, and glass fiber separator (Fisher Scientific), respectively. The cell was sealed in a glass chamber and then filled with 1 atm of high purity oxygen. All electrochemical measurements were performed using a Maccor battery cycler at 298 K. For the galvanostatic discharge/charge test, the lower and upper cutoff voltage is 2.3 and 4.5 V (vs. Li), respectively. To avoid the decomposition of electrolyte on the discharge products during the ORR/OER processes, the capacity-controlled electrochemical method that has been adopted in the literature is used in this work.[7,20] The capacity (mAh g^{-1}, based on the mass of carbon) of a Li−O_2 battery is determined by two parameters, the current density (I, mA g^{-1}) and discharge time (t, hour), in the range of 2.3−4.5 V. By changing I and t, the Li−O_2 cells with different discharged or recharged status were obtained, and the components and evolution of products on the cathode were characterized. The recharge capacity is less than or equal to the discharge capacity.

3. RESULTS AND DISCUSSION

3.1. Discharge Product Characterization. The first cycle discharge−charge voltage profiles of AC at 0.1 mA cm^{-2} (current over cathode area) are shown in Figure 1 with capacities of 250, 500, 700, and 1000 mA h g^{-1}. In each voltage profile in Figure 1, the charge capacity is the same as the discharge value. All discharged curves stay at about 2.7 V. The results for 1000 mA h g^{-1} show two distinct charge plateaus, one at 3.2−3.5 V and the other at ∼4.2 V, similar to that reported previously.[26] The other charge curves also show two distinct voltage plateaus, which are between 3.0 and 3.5 V and about 3.8 V and above. For example, the voltage profile at reversible capacity of 500 mA h g^{-1} (Figure 1b) shows an initial charge phase in which the voltage first ascends slightly from 3.0 to 3.5 V and then climbs rapidly above 4.0 V and keeps ascending slowly. In all cases in Figure 1, two distinct voltage plateaus during a complete reversible discharge−charge cycle always appear regardless of the capacity.

In order to determine the nature of the product on the discharged AC electrode, XRD characterization and Raman measurements were carried out. The Li−O_2 cell was discharged at 0.1 mA cm^{-2} and the capacity was 1200 mAh g^{-1}. The dried electrode was characterized with the use of XRD. The peaks from the discharge AC are identified as the (100), (101), and (110) peaks of Li_2O_2 according to the standard XRD histogram of Li_2O_2 (JCPDS No. 09-0355) as shown in Figure 2. The XRD patterns show broad diffraction peaks, which is consistent with previous reports.[1,3] The broad peaks may be attributed to poor crystallinity, perhaps due to disordered grain boundaries.

The Li−O_2 cell was discharged at 0.1 mA cm^{-2} for 1200 mAh g^{-1}, and the discharged AC cathode was characterized by micro-Raman measurement. The discharged-then-charged back to 3.5 V cathode was also measured. Since the LiO_2-like Raman band is more sensitive at low temperature based on our previous study, both spectra were measured at 100 K.[26] Several different spots (>5) of the surface were checked to ensure the

dx.doi.org/10.1021/ja403199d | J. Am. Chem. Soc. 2013, 135, 15364−15372

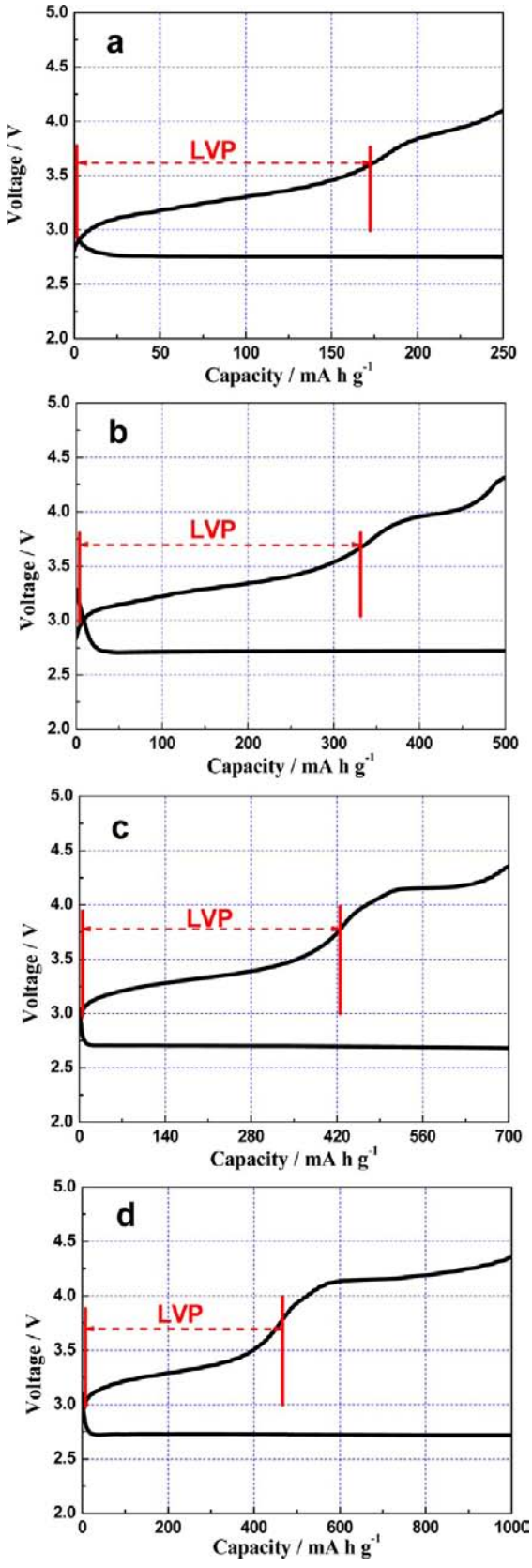

Figure 1. First galvanostatic discharge/charge curves of AC at 0.1 mA cm^{-2} with different capacities of (a) 250 mA h g^{-1}, (b) 500 mA h g^{-1}, (c) 700 mA h g^{-1}, and (d) 1000 mA h g^{-1}.

Raman spectra were reproducible. A typical Raman spectrum is shown in Figure 3. The discharged AC cathode shows a

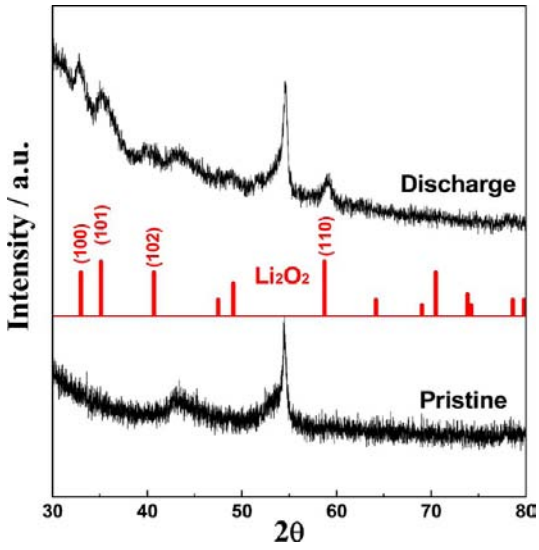

Figure 2. XRD spectra of pristine and discharged AC electrodes (capacity = 1200 mAh g^{-1}, I = 0.1 mA cm^{-1}) with a standard Li_2O_2 XRD histogram in the middle.

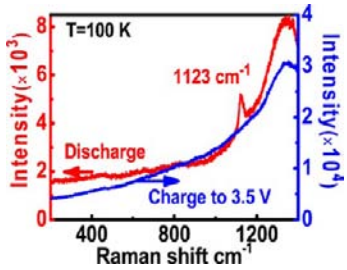

Figure 3. Raman spectrum of the discharged AC cathode surface showing graphite D (1330 cm^{-1}) and LiO_2-like bands (1123 cm^{-1} red trace). Raman spectrum of a similar AC cathode that was discharged and charged back to 3.5 V does not show the LiO_2-like band (blue trace). Both spectra were taken at 100 K.

prominent band (red trace) at 1123 cm^{-1} at 100 K consistent with a LiO_2-like species from both previous experimental results[2] and theory.[26] In our previous work,[26] a higher resolution ambient temperature Raman spectra shows the presence of broad weak peaks at 790 and 254 cm^{-1} consistent with the presence of Li_2O_2 (see also Figure S1 in Supporting Information). Others have also found the Raman peaks for Li_2O_2 to be broad.[4,20] This may be due to poor crystallinity or many thermodynamically closely related Li_2O_2 structures that statistically broaden the Raman peaks. Thus, the discharge products contain Li_2O_2 (XRD evidence) together with a LiO_2-like species (Raman evidence). The superoxide-like species is consistent with the magnetism that we previously reported for the discharge product on an AC cathode.[26] Finally, when the AC cathode is discharged (1200 mAh g^{-1}) and charged back to 3.5 V, it does not show a LiO_2-like band (blue trace). This is evidence that the LiO_2-like component decomposes below 3.5 V, although there may be some decomposition of Li_2O_2 below 3.5 V also.

Subsequently, we investigated the nature of the product being charged during the high voltage plateau. When the content of material to be tested is relatively low (generally less than 5%), the characteristic peaks of the material may not be detected by XRD. As the electrode contains carbon paper, AC, PVDF, and some products, the amount of products

dx.doi.org/10.1021/ja403199d | J. Am. Chem. Soc. 2013, 135, 15364−15372

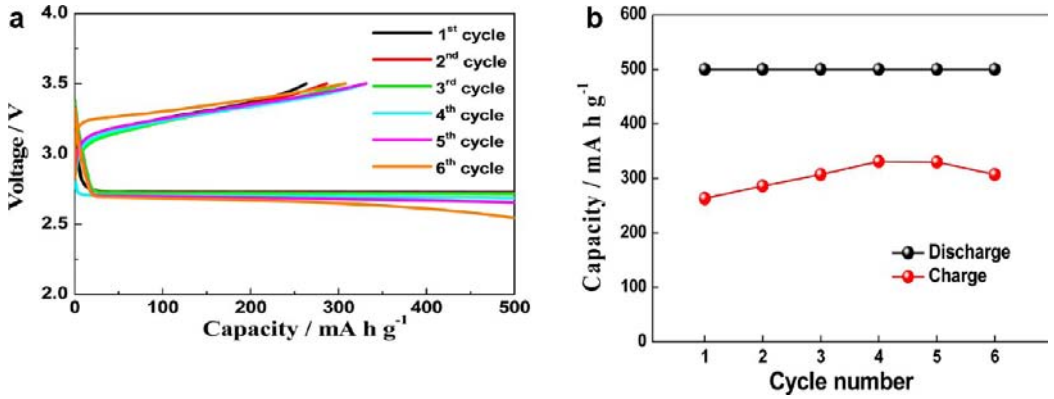

Figure 4. (a) Galvanostatic discharge/charge curves of AC. The cell was first discharged, and the capacity is ~500 mA h g^{-1}, and then it was charged back until 3.5 V. (b) Variation of discharge capacity and partially charged capacity on the number of cycles. The cell was first discharged, and the capacity is ~500 mA h g^{-1}, and then it was charged back until 3.5 V.

decomposing during the high voltage plateau is relatively small when the cell is discharged only once. To ensure sufficient material of the high plateau phase, we carried out the following procedure: (i) the cell was first discharged to the capacity of 500 mA h g^{-1}, and then was charged back to 3.5 V; (ii) according to the above procedure (i) repeat the cycle test for five more times and accumulate undecomposed products continuously on the surface of AC electrode. Figure 4a shows the discharge/charge curves for six cycles. With increasing cycle times, the discharge voltage profile drops from 2.75 to 2.55 V, probably because the accumulation of undecomposed products on the surface leads to an increase of the overpotential.[12] The reversible charged capacity increases gradually up to the fourth cycle and then begins to fade, as shown in Figure 4b. After six cycles, the estimated capacity of the deposits on the AC electrode was about 1170 mA h g^{-1}. The dried electrode was characterized by XRD, and the results are shown in Figure 5.

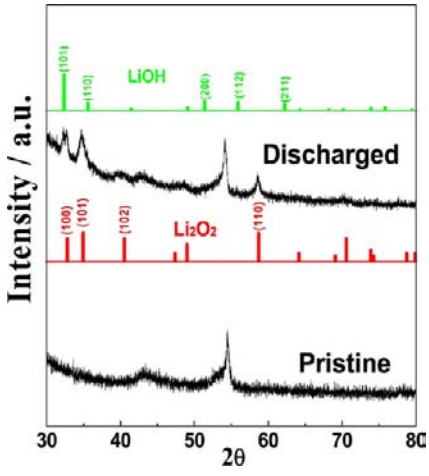

Figure 5. XRD spectra of pristine and discharge AC electrode after six cycles.

The peaks (100), (101), and (110) related to Li_2O_2 are clearly evident in the XRD pattern. Therefore, this provides strong evidence that the product that decomposes above 3.5 V is a Li_2O_2 phase. The (100) peak at ~32.5° now contains a notable shoulder peak that is likely to belong to the (101) peak of lithium hydroxide (LiOH). This could be explained by the theory that Nazar put forward in which superoxide species with the help of a catalyst readily de-hydrofluorinated PVDF to give byproducts, containing H_2O_2 which then decomposed and produced H_2O, and the generated Li_2O_2 readily reacted with H_2O to form LiOH.[1] Thus, a small amount of LiOH was generated after this lengthy procedure (Figure 4) in order to build up a sufficient amount of Li_2O_2 in the higher voltage plateau for the XRD measurement.

Thus, on the basis of the characterization data, the discharge product exhibits a superoxide-like character as well as evidence for the presence of Li_2O_2. The superoxide character disappears after the charge reaches 3.5 V, suggesting that a phase with an oxygen-rich superoxide-like character is related to the first plateau and that Li_2O_2 is correlated with the second plateau. The exact nature of the oxygen-rich component is unknown. In the next section, we present an investigation of the kinetics based on the dependence of the lengths of the two plateaus on charge capacity and charge density.

3.2. Kinetics Study of the Discharge Product Composition. We have carried out measurements of the dependence of the lower charge plateau on capacity (time) for a kinetics analysis of the likely composition of the discharge product. For this analysis, we assume that some type of solid LiO_2 forms in the discharge process initially as a one-electron process (i.e., $n(Li^+ + e^- + O_2) \rightarrow LiO_2(s)$), and disproportionation leads to solid Li_2O_2 (i.e., $LiO_2(s) \rightarrow Li_2O_2(s) + O_2$). The disproportionation reaction is kinetically controlled so that $LiO_2(s)$ will be converted to $Li_2O_2(s)$ over time, as opposed to a two-electron process in which Li_2O_2 forms directly. If this occurs, the discharge product will be composed of two components: Li_2O_2 and the remaining "LiO_2". The exact nature of such a two-phase system is unclear. However, Shao-Horn et al.[31] in their Li–O_2 work have envisioned such a product to consist of core–shell system with the core being Li_2O_2 and the shell being oxygen-rich superoxide-like. Nazar et al.[32] have also provided evidence that a discharge product in some of their Li–O_2 cells can have an oxygen-rich component. In a previous paper, we have presented calculations of an oxygen-rich Li_2O_2 surface that represents such a two-component system.[26] We have also carried out calculations on a small nanoparticle to illustrate a $(Li_2–xO_2)n$ core–shell structure that could be part of the initial one-electron growth process (see Figure S2, Supporting Information).

The low voltage plateaus shown in Figure 1 are used to investigate the kinetics involving the discharge product. In

dx.doi.org/10.1021/ja403199d | J. Am. Chem. Soc. 2013, 135, 15364–15372

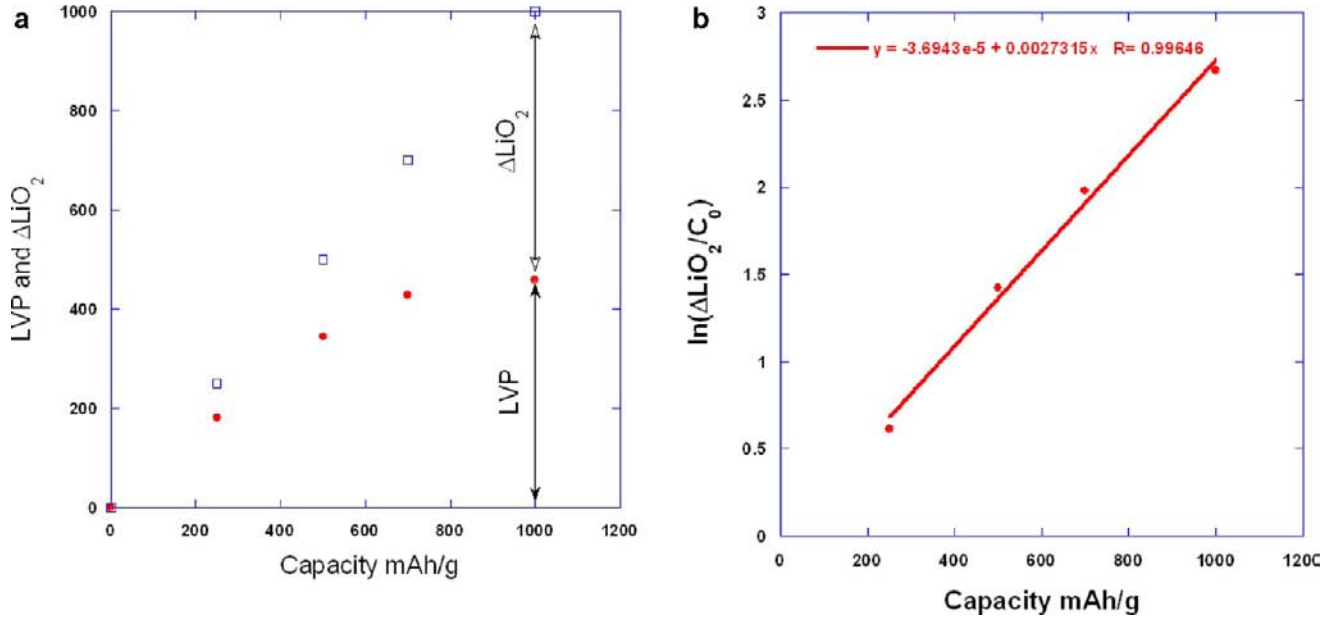

Figure 6. (a) The LVP portions extracted from Figure 1 are plotted against the discharge capacity (red circles). The blue squares are the discharge capacity and ΔLiO_2 = total discharge capacity - LVP. (b) Natural log function of the disappearance of the "LiO_2/C_0" component (from panel a) plotted against the capacity (Q) showing a linear correlation resulting from a first-order reaction.

order to determine whether the data in Figure 1 are consistent with the one-electron type of reaction mechanism discussed above, we assume a correlation of the first charge plateau with the oxygen-rich discharge product remaining from partial disproportionation to Li_2O_2. As the analysis described below shows, this assumption is consistent with the data. The amount of the low voltage plateau (LVP) can be derived by taking the derivative of the charge profile curves from Figure 1 (see Figure S3, Supporting Information). In an ideal situation, the Li metal anode electrochemical discharge surface reaction ($Li \rightarrow Li^+/e^-$) is a zero-order reaction; i.e., the reaction rate is a constant and independent of the Li concentration. If all the electrons are used to generate oxygen anion (O_2^- eq 3) and then LiO_2 (eq 4), the theoretical maximum amount of the oxygen-rich component that can be generated will be equal to the discharge capacity, Q, plotted as blue squares in Figure 6a. Assuming the oxygen-rich component is similar to LiO_2, it would disproportionate (eq 5) as a function of time and/or capacity Q (Q (mAh g^{-1}) = I (mA g^{-1}) × t (h)) under constant current conditions for a specific electrode (constant weight). The LVP portions from Figure 1 are plotted against the discharge capacity (red circles Figure 6a). The difference between the maximum possible amount (total discharge capacity, blue squares) and the actual remaining amount (LVP, red circles) is the $\Delta(LiO_2)$. The LiO_2 disproportionation reaction (eq 5) is a first-order reaction.[2] For a first-order reaction: A → P, where A is the reactant and P product, the reaction rate is

$$r = \frac{-\mathrm{d}[\mathrm{A}]}{\mathrm{d}t} = k[\mathrm{A}] \tag{6}$$

and the integrated first-order rate law is[33]

$$\ln[\mathrm{A}] = -kt + C \text{ or } \ln\frac{[\mathrm{A}]}{C_0} = -kt \tag{7}$$

where k is the rate constant, t time, and C and C_0 are fitting constants. For the four discharge reactions in Figure 1, each discharge capacity is different; therefore, we cannot directly apply eq 7 that describes reactant concentration as a function of time for a single reaction. However, for the four discharge/charge curves in Figure 1, one can monitor the disappearance of LiO_2 (i.e., ΔLiO_2 = total discharge capacity − LVP; see Figure 6a) as a function of time or capacity. A fitting constant C_0 is applied here so that $[A]/C_0$ is unitless and $\ln([A]/C_0)$ can be plotted properly. When the $\Delta LiO_2/C_0$ is plotted against the capacity (Q), a good linear correlation is observed as seen in Figure 6b. The $\Delta(LiO_2)$ corresponds to the disappearance of reactant A or the growth of product P, which gives the positive slope. Therefore, the disappearance of the oxygen-rich component in the $Li-O_2$ cell (ΔLiO_2) indeed follows a first-order reaction, consistent with a one-electron reaction and some fraction of disproportionation. Thus, the analysis confirms that the first charging plateaus observed in Figure 1 is associated with the oxygen-rich component.

We have also investigated the existence of a disproportionation reaction in the discharge process by examining the dependence of the two plateaus on the current density. From eqs 6 and 7, it is expected that the amount of the oxygen-rich and the Li_2O_2 components will be sensitive to current density. As shown in Figure 7, three cells are discharged with current densities of 0.05, 0.1, and 0.2 mA cm^{-2} with the same discharge capacity of 1000 mA h g^{-1}. And then they are charged back with the same current density of 0.1 mA cm^{-2} with the same capacity. The lower voltage plateaus for these three voltage curves are clearly different. When the cell is discharged at 0.05 mA cm^{-2} (red curve), the low voltage plateau is the shortest, which means that the fraction of oxygen-rich superoxide component of the total discharge capacity is the smallest. On the contrary, at the discharge current of 0.2 mA cm^{-2} (green curve), the low voltage plateau is longest, which indicates the fraction of oxygen-rich component of the total discharge capacity is the largest. Therefore, there is less disproportionation (decomposition of LiO_2) at high current densities (shorter times) and more disproportionation at low current densities (longer times). This is consistent with the evidence from

dx.doi.org/10.1021/ja403199d | J. Am. Chem. Soc. 2013, 135, 15364−15372

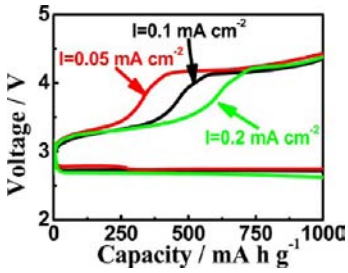

Figure 7. Discharge/charge curves of AC with different discharge current density and the same charge current density. The red curve is the discharge current of 0.05 mA cm^{-2} and charge current of 0.1 mA cm^{-2}; the black curve is the discharge current of 0.1 mA cm^{-2} and charge current of 0.1 mA cm^{-2}; the green curve is the discharge current of 0.2 mA cm^{-2} and charge current of 0.1 mA cm^{-2}. See Figure S9 for SEM images of toroids at current density of 0.2 mA cm^{-2}.

variation of the charge capacity where with longer discharge time more disproportionation occurs with the oxygen-rich component being a smaller fraction of the total capacity. This is also consistent with the observation of Nazar et al.,[1,32] who have reported that higher current densities result in more growth via LiO_2. As the current density is increased, there is increased LiO_2 generation and nucleation due to faster electron transfer and, thus, larger amounts of "LiO_2"-like content.

The conclusions from the kinetics analysis are reinforced by other evidence. (1) The Raman spectra indicates that the LiO_2-like component disappears when charged to 3.5 V, consistent with the kinetics analysis. This is shown in Figure 3 (blue trace) where, when the AC cathode is discharged (to 1200 mAh g^{-1}) and charged back to 3.5 V, the LiO_2-like band disappears. (2) The Raman and XRD data presented in the previous section indicate that both superoxide and Li_2O_2 components are in the discharge product, again consistent with the kinetics analysis. (3) In previous work,[26] we found that the intensity of the magnetic phase transition from the superoxide increases with discharge capacity for the AC cathode, which is in agreement with the kinetics analysis that the amount of oxygen-rich superoxide component (see Figure 6a) increases with increasing capacity (although the fraction of total capacity that is oxygen-rich component decreases). (4) Finally, an analysis of the data from different current densities (see Figure S4 in the Supporting Information) also shows that the lower plateau is consistent with a one-electron reaction and partial disproportionation, similar to what was found in the analysis of the discharge capacity data.

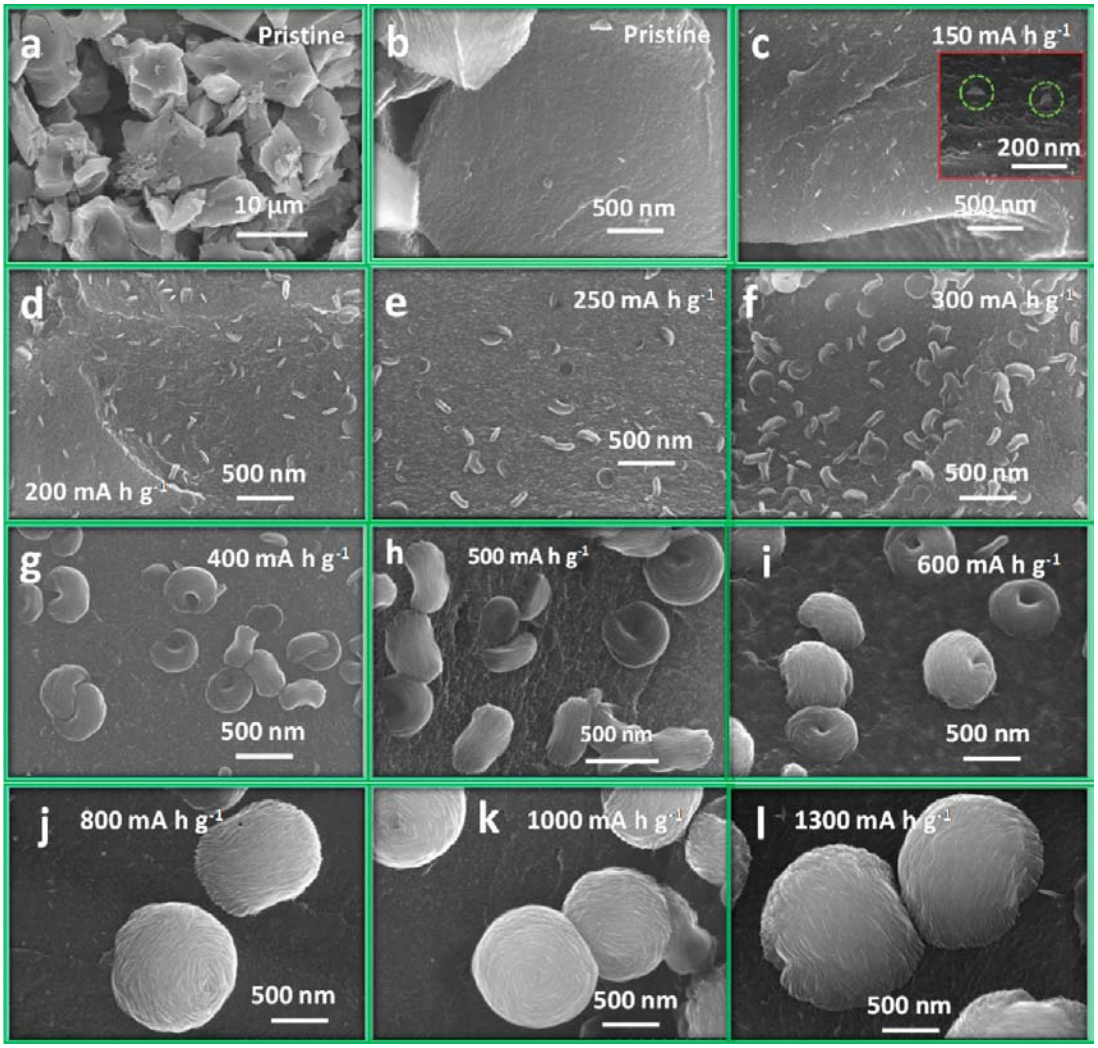

Figure 8. The morphologic growth process of LiO_2-like species/Li_2O_2 composites at different discharge capacities of (a, b) pristine, (c) 150, (d) 200, (e) 250, (f) 300, (g) 400, (h) 500, (i) 600, (j) 800, (k) 1000, and (l) 1300 mA h g^{-1}.

dx.doi.org/10.1021/ja403199d | J. Am. Chem. Soc. 2013, 135, 15364−15372

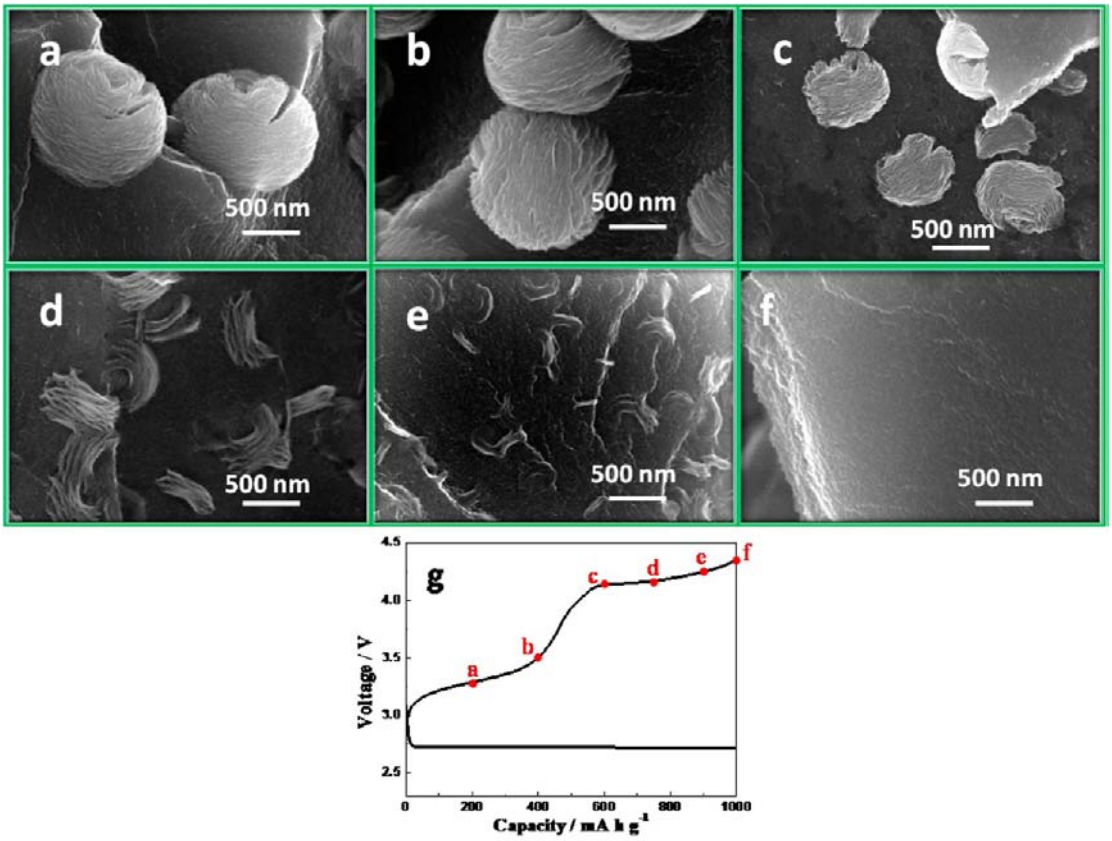

Figure 9. The morphologic decomposition process of LiO_2-like species/Li_2O_2 composites at different charge capacities after a discharge capacity of 1000 mA h g^{-1}: (a) 200, (b) 400, (c) 600, (d) 750, (e) 900 and 1000 mA h g^{-1}. (g) Voltage profile during reversible charge after discharge and the red dots represent different charged capacity.

Thus, this kinetics study provides evidence that the lithium peroxide discharge product in this Li−O_2 battery based on AC as the cathode material is a composite of an oxygen-rich component with superoxide-like character and a Li_2O_2 component resulting from a disproportionation reaction of the superoxide component. This result is consistent with a slow rate of disproportionation obtained from analysis of the four different capacity runs (see Figure S10, Supporting Information), which gives a half-life of about 8 h for lithium superoxide. The porosity of the activated carbon can provide an oxygen-rich environment[34,35] and a large number of active sites for oxygen reduction.[36] This can facilitate oxygen mass transport and oxygen reduction that likely promotes the rate of growth of the superoxide discharge product resulting in the oxygen-rich component indicated by the kinetics analysis. In the next section, we present results of the morphological evolution of the lithium peroxide and how it relates to this composite.

3.3. Morphological Evolution of Discharge/Charge Product. To capture the details of morphological changes during discharge, a set of cells was discharged with different fixed capacity at 0.1 mA cm^{-2} and then observed through SEM imaging as shown in Figure 8. The discharged electrode was washed with TEGDME solvent and dried at 80 °C under a vacuum before SEM observation. Figure 8a,b shows the pristine surface of AC electrode before discharge. The AC particles range from a few to tens of micrometers and the surface of the particles is very clear. The surface area of AC is up to 3840 m^2 g^{-1}, and the dominant pores are distributed at about 1 and 3 nm (shown in Figure S5, Supporting Information). When the discharge capacity is ∼150 mA h g^{-1}, there are small deposits on the AC surface (Figure 8c). At the discharge capacity of ∼200 mA h g^{-1}, the partial toroidal morphology of the deposits first becomes evident (Figure 8d). The toroids increase in size with increasing discharge capacity (Figure 8e−g). As the discharge capacity increases from 500 to 1300 mA h g^{-1} (Figure 8h−l), the diameter of the toroids increases from ∼600 to ∼1500 nm, and the shape of the toroids evolves from "ring torus" to spherical-like toroids (i.e., with a spiral hole at both poles). In order to further characterize the nature of the toroids, EDX measurements of the pristine AC electrode and the discharged electrode with the capacity of ∼800 mA h g^{-1} were carried out (shown in Figures S6−S8). The EDX results show a predominance of oxygen in the toroids consistent with the presence of Li_2O_2 or LiO_2-like species. Here it is noteworthy to point out that the experimental observation of toroid discharge products has been reported recently based on different carbon-based electrodes,[1,3,14,37,38] although not in as much detail. To account for the presence of toroidal morphology of Li_2O_2 deposits, a speculative mechanism has been proposed, which is based on the assembly of Li_2O_2 nanoparticles in the electrolyte solution.[1]

To track the morphological evolution of the reaction product at different stages of the charging process, cells were separately discharged to the same initial capacity of 1000 mA h g^{-1} and then charged back sequentially from low to high capacity with fixed current density at 0.1 mA cm^{-2}. The morphological evolution is shown by stage a−f in Figure 9, and the voltage profile at different charge stages is indicated in Figure 9g. The AC electrode was washed with TEGDME solvent and dried at 80 °C under a vacuum and then characterized by SEM imaging.

dx.doi.org/10.1021/ja403199d | J. Am. Chem. Soc. 2013, 135, 15364−15372

Comparing Figure 9, panel a (charged back to 200 mAh g^{-1}) with Figure 9k (discharged to 1000 mAh g^{-1}), the toroid morphology remains but appears to be more textured on the surface with what appears to be grain boundaries. When the charge capacity is increased to 400 mA h g^{-1} with the voltage close to 3.5 V, the size of the toroids remain approximately the same; however, surface texture becomes more pronounced (Figure 9b), which might be attributed to the decomposition of an oxygen-rich "LiO_2"-like component that occurs during the first plateau from the grain boundaries and surface. As the charge capacity approaches 600 mA h g^{-1} with charge voltage larger than 3.5 V, the morphology of the objects appears to be "ring-toroid"-like, but the size of these discharge product particles are significantly reduced, i.e., from ∼1500 to 600 nm in Figure 9c. Subsequently, when the charged capacity is 750 mA h g^{-1}, the traces of toroid particles with size ∼250 to 500 nm still can be seen; however, the compactness is substantially lost as shown in Figure 9d. At a capacity of 900 mA h g^{-1} with a charging voltage ≈ 4.0−4.2 V, the remains of the initially discharge product particles shrink (Figure 9e). Consequently, when the charge capacity becomes equal to the discharge capacity (i.e., 1000 mA h g^{-1}), the SEM image shows that the all the particles are completely decomposed, and the pristine surface of the AC electrode is recovered (Figure 9f) similar to Figure 8b.

Thus, the morphological evolution during a complete discharge−charge cycle performed under a "capacity-controlled" condition indicates several important things about the oxygen-rich/Li_2O_2 composites. First, the evolution of the toroids revealed by the SEM images during discharge differs significantly from those during charge, which suggests that the formation and decomposition mechanisms are different. This is consistent with the kinetics study that there is a chemical transformation (disproportionation) occurring during discharge, which cannot occur during charge. Second, during charge the decomposition appears to occur from grain boundaries and outer portions of the toroids initially, which suggests the location of oxygen-rich component since decomposition of the oxygen-rich component occurs during the first charge plateau. The lower charge potential results are consistent with studies by Bruce et al.,[2] who reported that OER for LiO_2 has a lower charge potential, and Lu and Shao-Horn who reported that a Li-deficient (oxygen-rich) part of lithium peroxide has a lower charge potential than that of bulk Li_2O_2.[39] A lower first plateau has also been observed by others such as Nazar et al. in Li−O_2 cell using a Co_3O_4 catalyst.[25]

4. CONCLUSIONS

The following conclusions can be drawn from this work on a Li−O_2 battery using a large surface area activated carbon and an ether-based electrolyte:

(1) Two components, an oxygen-rich component with superoxide-like character and a Li_2O_2 component, have been identified in the discharge product. The superoxide-like character disappears at the end of the first plateau suggesting that the oxygen-rich component has a significantly lower charge potential than the Li_2O_2 component charge. A recent theoretical study[40] has also suggested that oxygen-rich Li_2O_2 could have a low charge overpotential, consistent with these results.

(2) A kinetics study based on the capacity and charge density dependence of the charge plateaus provides evidence for a first-order reaction during discharge from the oxygen-rich superoxide-like component to the Li_2O_2 component due to LiO_2 disproportionation. This further points to a discharge product with the two types of domains. The porosity of the activated carbon provides an environment that likely promotes growth of this type of composite discharge product.

(3) The different evolution of the toroids during discharge and charge suggests that the formation and decomposition mechanisms are different, consistent with the kinetics analysis showing superoxide disproportionation. Also the evolution during charge suggests that the oxygen-rich domain is in the grain boundaries and outer parts of the toroids.

The results of this study indicate that activated carbon could be the basis for development of advanced cathode material for Li−O_2 batteries as it affords new possibilities to control of the nature of the discharge product via the disproportionation reaction and addition of electrocatalysis functionality. Further development of the activated cabon cathode is also needed to improve cycling as it degrades as reported previous[26] possibly due to pore clogging or electrolyte decomposition on carbon or discharge product surfaces.

■ ASSOCIATED CONTENT

Supporting Information

Additional information is provided on (a) Raman data for Li_2O_2 and LiO_2, (b) DFT calculations of core−shell oxygen-rich Li_2O_2 systems, (c) kinetics analysis of capacity data, (d) pore size distribution of the activated carbon, (e) EDX spectrum of the discharged cathode, and (f) additional SEM images of toroids. This material is available free of charge via the Internet at http://pubs.acs.org.

■ AUTHOR INFORMATION

Corresponding Authors

curtiss@anl.gov
amine@anl.gov

Notes

The authors declare no competing financial interest.

■ ACKNOWLEDGMENTS

Research at Argonne National Laboratory was funded by the U.S. Department of Energy, Joint Center for Energy Storage Research and Vehicle Technologies Office under Contract No. DE-AC02-06CH11357 by UChicago Argonne, LLC. The electron microscopy measurement was accomplished at the Electron Microscopy Center for Materials Research, and the Raman measurements were performed at the Center for Nanoscale Materials at Argonne National Laboratory. We also acknowledge helpful discussions with Professor Linda Nazar.

■ REFERENCES

(1) Black, R.; Oh, S. H.; Lee, J. H.; Yim, T.; Adams, B.; Nazar, L. F. *J. Am. Chem. Soc.* **2012**, *134*, 2902.
(2) Peng, Z. Q.; Freunberger, S. A.; Hardwick, L. J.; Chen, Y. H.; Giordani, V.; Barde, F.; Novak, P.; Graham, D.; Tarascon, J. M.; Bruce, P. G. *Angew. Chem., Int. Ed.* **2011**, *50*, 6351.
(3) Mitchell, R. R.; Gallant, B. M.; Thompson, C. V.; Shao-Horn, Y. *Energy Environ. Sci.* **2011**, *4*, 2952.
(4) Abraham, K. M.; Jiang, Z. *J. Electrochem. Soc.* **1996**, *143*, 1.
(5) Du, P.; Lu, J.; Lau, K. C.; Luo, X.; Bareno, J.; Zhang, X.; Ren, Y.; Zhang, Z.; Curtiss, L. A.; Sun, Y.-K.; Amine, K. *Phys. Chem. Chem. Phys.* **2013**, *15*, 5572−5581.
(6) Assary, R. S.; Lu, J.; Du, P.; Luo, X.; Zhang, X.; Ren, Y.; Curtiss, L. A.; Amine, K. *ChemSusChem* **2013**, *6*, 51.

(7) Jung, H.-G.; Hassoun, J.; Park, J.-B.; Sun, Y.-K.; Scrosati, B. *Nat. Chem.* **2012**, *4*, 579.
(8) Xiao, J.; Mei, D. H.; Li, X. L.; Xu, W.; Wang, D. Y.; Graff, G. L.; Bennett, W. D.; Nie, Z. M.; Saraf, L. V.; Aksay, I. A.; Liu, J.; Zhang, J. G. *Nano Lett.* **2011**, *11*, 5071.
(9) McCloskey, B. D.; Scheffler, R.; Speidel, A.; Bethune, D. S.; Shelby, R. M.; Luntz, A. C. *J. Am. Chem. Soc.* **2011**, *133*, 18038.
(10) McCloskey, B. D.; Bethune, D. S.; Shelby, R. M.; Girishkumar, G.; Luntz, A. C. *J. Phys. Chem. Lett.* **2011**, *2*, 1161.
(11) Freunberger, S. A.; Chen, Y. H.; Peng, Z. Q.; Griffin, J. M.; Hardwick, L. J.; Barde, F.; Novak, P.; Bruce, P. G. *J .Am. Chem. Soc.* **2011**, *133*, 8040.
(12) Freunberger, S. A.; Chen, Y. H.; Drewett, N. E.; Hardwick, L. J.; Barde, F.; Bruce, P. G. *Angew. Chem., Int. Ed.* **2011**, *50*, 8609.
(13) Ottakam Thotiyl, M. M.; Freunberger, S. A.; Peng, Z.; Bruce, P. G. *J .Am. Chem. Soc.* **2013**, *135*, 494.
(14) Wang, Z.-L.; Xu, D.; Xu, J.-J.; Zhang, L.-L.; Zhang, X.-B. *Adv. Funct. Mater.* **2012**, *22*, 3699.
(15) Shitta-Bey, G. O.; Mirzaeian, M.; Halla, P. J. *J. Electrochem. Soc.* **2012**, *159*, A315.
(16) Trahey, L.; Karan, N. K.; Chan, M. K. Y.; Lu, J.; Ren, Y.; Greeley, J.; Balasubramanian, M.; Burrell, A. K.; Curtiss, L. A.; Thackeray, M. M. *Adv. Energy Mater.* **2013**, *3*, 75.
(17) Shui, J. L.; Karan, N. K.; Balasubramanian, M.; Li, S. Y.; Liu, D. J. *J .Am. Chem. Soc.* **2012**, *134*, 16654.
(18) Lee, J.-H.; Black, R.; Popov, G.; Pomerantseva, E.; Nan, F.; Botton, G. A.; Nazar, L. F. *Energy Environ. Sci.* **2012**, *5*, 9558.
(19) Lu, Y. C.; Kwabi, D. G.; Yao, K. P. C.; Harding, J. R.; Zhou, J. G.; Zuin, L.; Shao-Horn, Y. *Energy Environ. Sci.* **2011**, *4*, 2999.
(20) Peng, Z. Q.; Freunberger, S. A.; Chen, Y. H.; Bruce, P. G. *Science* **2012**, *337*, 563.
(21) McCloskey, B. D.; Scheffler, R.; Speidel, A.; Girishkumar, G.; Luntz, A. C. *J. Phys. Chem. C* **2012**, *116*, 23897.
(22) Hummelshoj, J. S.; Blomqvist, J.; Datta, S.; Vegge, T.; Rossmeisl, J.; Thygesen, K. S.; Luntz, A. C.; Jacobsen, K. W.; Norskov, J. K. *J. Chem. Phys.* **2010**, *132*, 071101.
(23) Laoire, C. O.; Mukerjee, S.; Abraham, K. M.; Plichta, E. J.; Hendrickson, M. A. *J. Phys. Chem. C* **2010**, *114*, 9178.
(24) Laoire, C. O.; Mukerjee, S.; Abraham, K. M.; Plichta, E. J.; Hendrickson, M. A. *J. Phys. Chem. C* **2009**, *113*, 20127.
(25) Black, R.; Lee, J. H.; Adams, B.; Mims, C. A.; Nazar, L. F. *Angew. Chem., Int. Ed.* **2013**, *52*, 392.
(26) Yang, J.; Zhai, D.; Wang, H.-H.; Lau, K. C.; Schlueter, J. A.; Du, P.; Myers, D. J.; Sun, Y.-K.; Curtiss, L. A.; Amine, K. *Phys. Chem. Chem. Phys.* **2013**, *15*, 3764.
(27) Radin, M. D.; Rodriguez, J. F.; Tian, F.; Siegel, D. J. *J .Am. Chem. Soc.* **2012**, *134*, 1093.
(28) Lau, K. C.; Assary, R. S.; Redfern, P.; Greeley, J.; Curtiss, L. A. *J. Phys. Chem. C* **2012**, *116*, 23890.
(29) Seaton, N. A.; Walton, J. P. R. B.; Quirke, N. *Carbon* **1989**, *27*, 853.
(30) Zhang, Z. C.; Lu, J.; Assary, R. S.; Du, P.; Wang, H. H.; Sun, Y. K.; Qin, Y.; Lau, K. C.; Greeley, J.; Redfern, P. C.; Iddir, H.; Curtiss, L. A.; Amine, K. *J. Phys. Chem. C* **2011**, *115*, 25535.
(31) Gallant, B. M.; Kwabi, D. G.; Mitchell, R. R.; Zhou, J.; Thompson, C. V.; Shao-Horn, Y. *Energy Environ. Sci.* **2013**, *6*, 2518−2528.
(32) Adams, B. D.; Radtke, C.; Black, R.; Trudeau, M. L.; Zaghib, K.; Nazar, L. F. *Energy Environ. Sci.* **2013**, *6*, 1772.
(33) Moore, W. J. *Physical Chemistry*; Prentice Hall, Inc.: Englewood Cliffs, NJ, 1972; pp 333−333.
(34) Kaneko, K. Nanodimensional Magnetic Assembly of Confined O_2. In *Surfaces of Nanoparticles and Porous Materials*; Schwarz, J. A., Contescu, C. I., Eds.; Surfactant Science Series, Vol. *78*; Marcel Dekker: New York, 1999.
(35) Kobayashi, N.; Enoki, T.; Ishii, C.; Kaneko, K.; Endo, M. *J. Chem. Phys.* **1998**, *109*, 1983.
(36) Qu, D. *Carbon* **2007**, *45*, 1296.
(37) Shao, Y.; Ding, F.; Xiao, J.; Zhang, J.; Xu, W.; Park, S.; Zhang, J.-G.; Wang, Y.; Liu, J. *Adv. Funct. Mater.* **2013**, *23*, 987.
(38) Jung, H.-G.; Kim, H.-S.; Park, J.-B.; Oh, I.-H.; Hassoun, J.; Yoon, C. S.; Scrosati, B.; Sun, Y.-K. *Nano Lett.* **2012**, *12*, 4333.
(39) Lu, Y. C.; Shao-Horn, Y. *J. Phys. Chem. Lett.* **2013**, *4*, 93.
(40) Kang, S. Y.; Mo, Y.; Ong, S. P.; Ceder, G. *Chem. Mater.* **2013**, *25*, 3328.